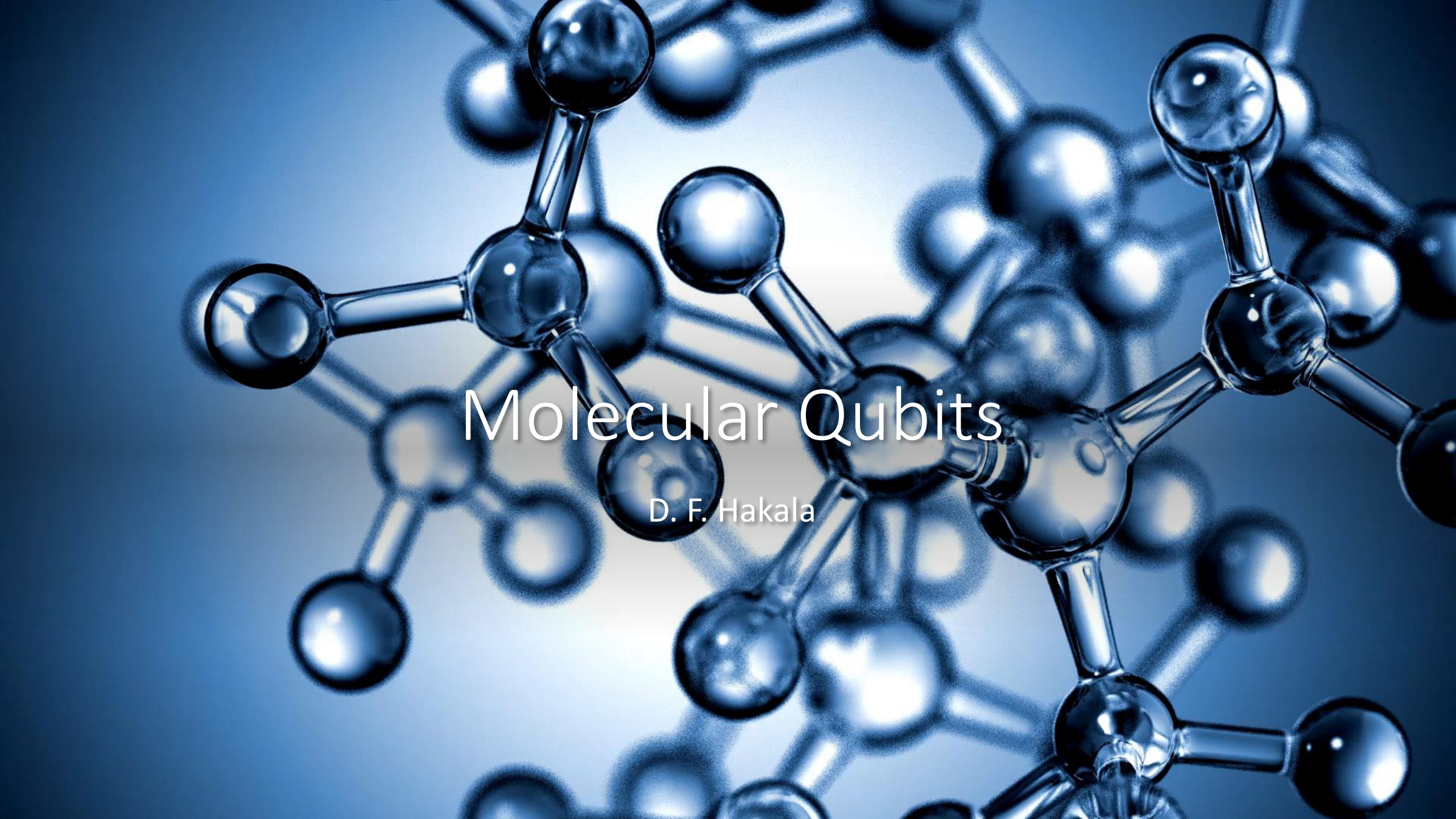

Molecular Qubits

D. F. Hakala

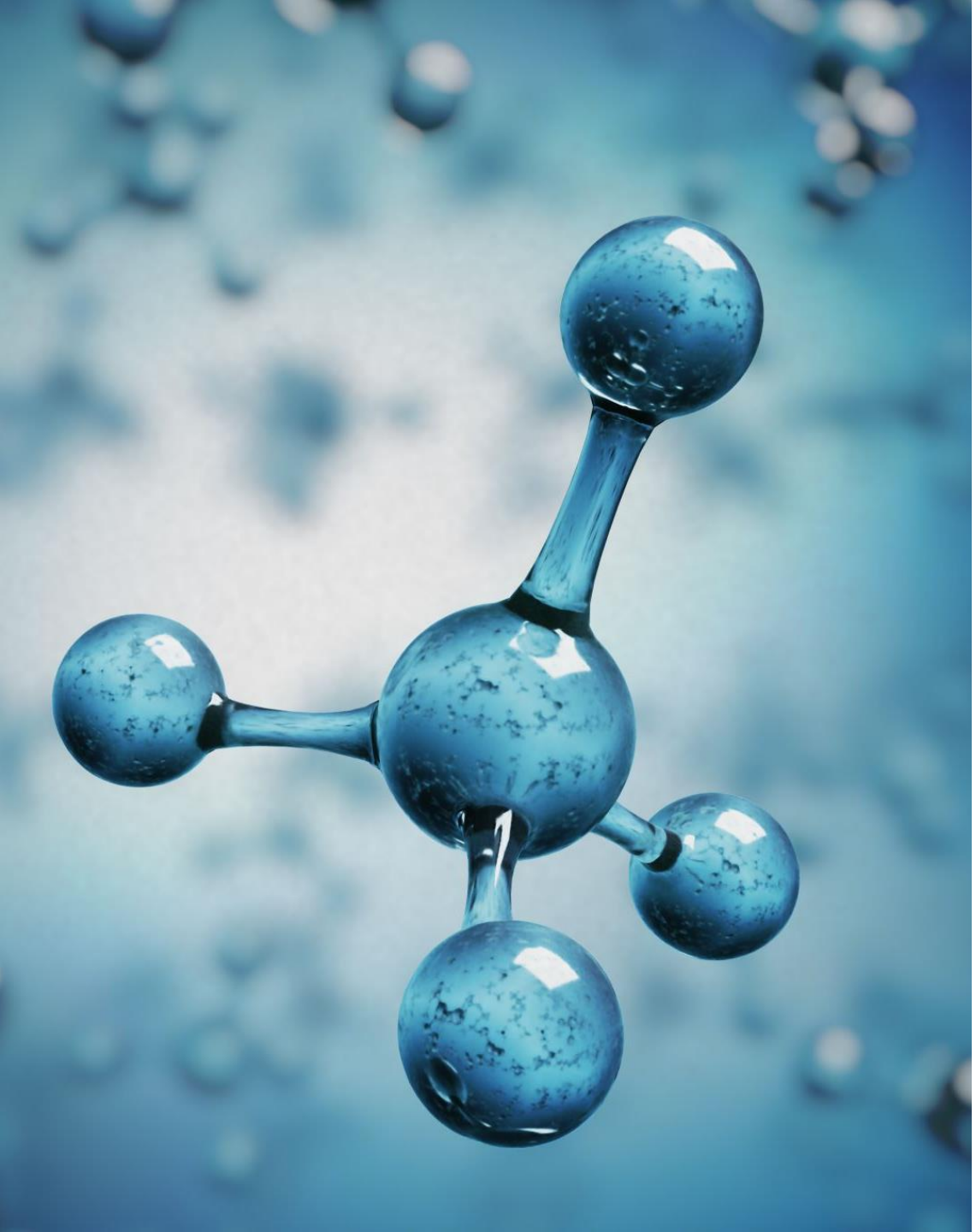

Introduction-Molecular Qubits

- A good relatively recent review related to molecular qubits is
- **Recent Innovations in Solid-State and Molecular Qubits for Quantum Information Applications**

  J. Phys. Chem. Lett. 2021, 12, 10742-10745
- There are over 40 references in this article, many of them with respect to molecular qubits.
- This is an overview for a Virtual Issue of J. Phys .Chem.Lett. on this subject.

Bloch Sphere Representation of the Qubit

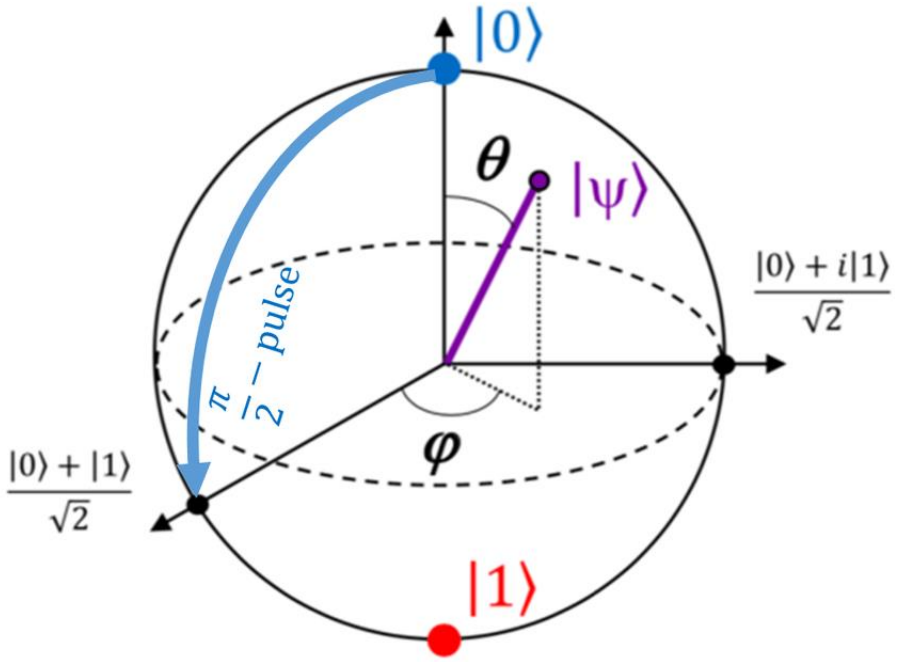

$$|\psi\rangle = cos\frac{\theta}{2}|0\rangle + e^{i\varphi}sin\frac{\theta}{2}|1\rangle$$

Applying (typically) microwave pulses of the correct time and frequency(it will need to be at the resonance of the energy difference between the |0> and |1> states at the applied magnetic field strength) will rotate the qubit from its initial orientation to a final one.

Assume the qubit is initially in the |0> state (theta =0). A resonant frequency pulse of theta=Pi/2 will rotate the qubit 90 degrees on the block sphere and result in a superposition (equal weights) of the |0> and |1> states or a normalized state of $(|0\rangle+|1\rangle)/2^{1/2}$. A pulse of length theta=Pi would change the qubit from the |0> state to the |1> state, effectively a NOT gate.

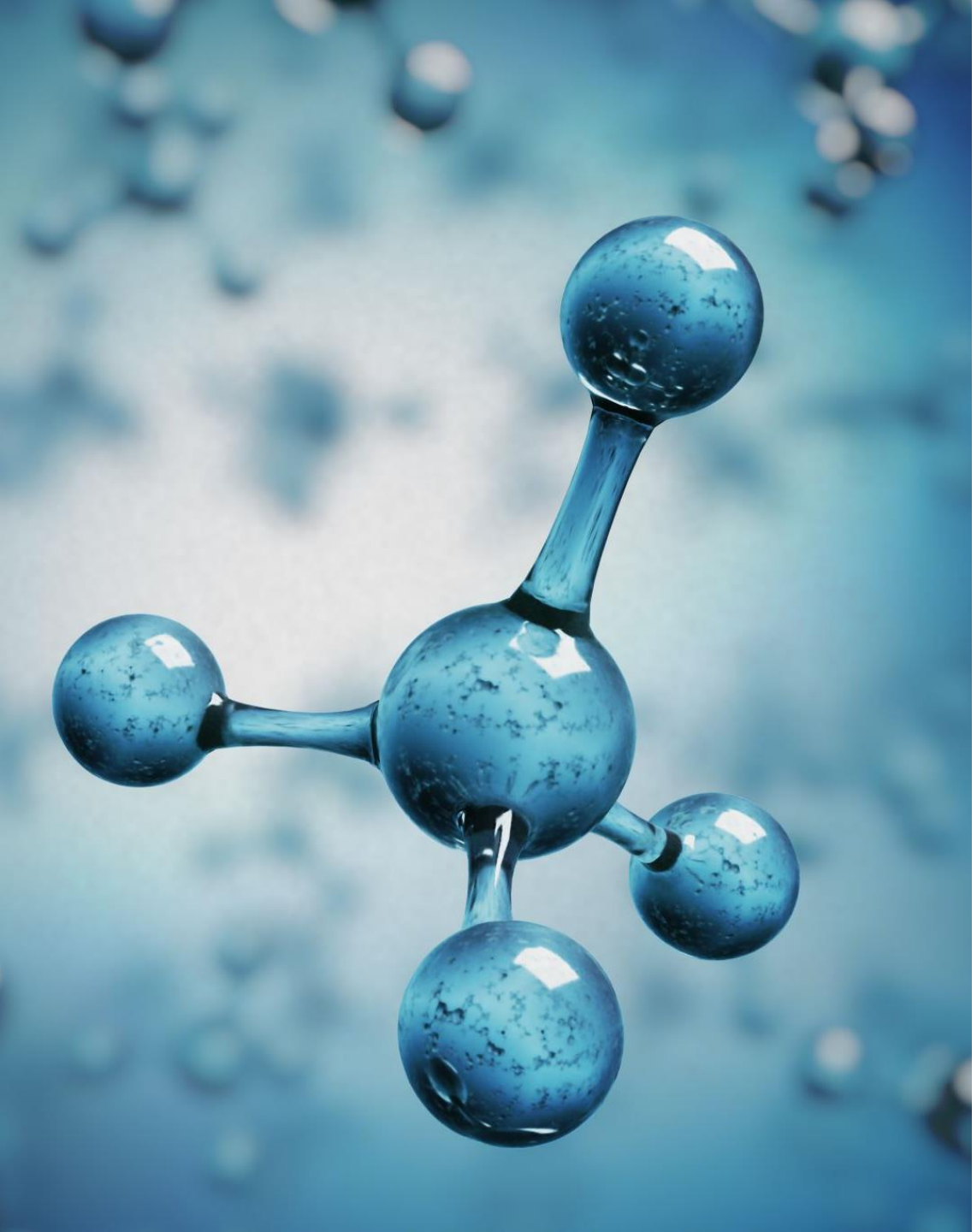

Molecular Qubits

- A qubit is an object that has two states (generally referred to as |0> and |1>) and all their superpositions. There are many possible physical implementations of the qubit. One of these that is attractive is the molecular qubit.
- The attractiveness is for several reasons.
  - They are small which will help in scaling up to higher device densities
  - They can be engineered or designed with respect to a number of different properties.
  - They are capable of being encoded, addressed, and read by means such as optical or microwave radiation.
- A typical molecular qubit is one that is spin based using the spin of unpaired electron(s). This energy of the molecule will both change and split in response to an applied magnetic field.

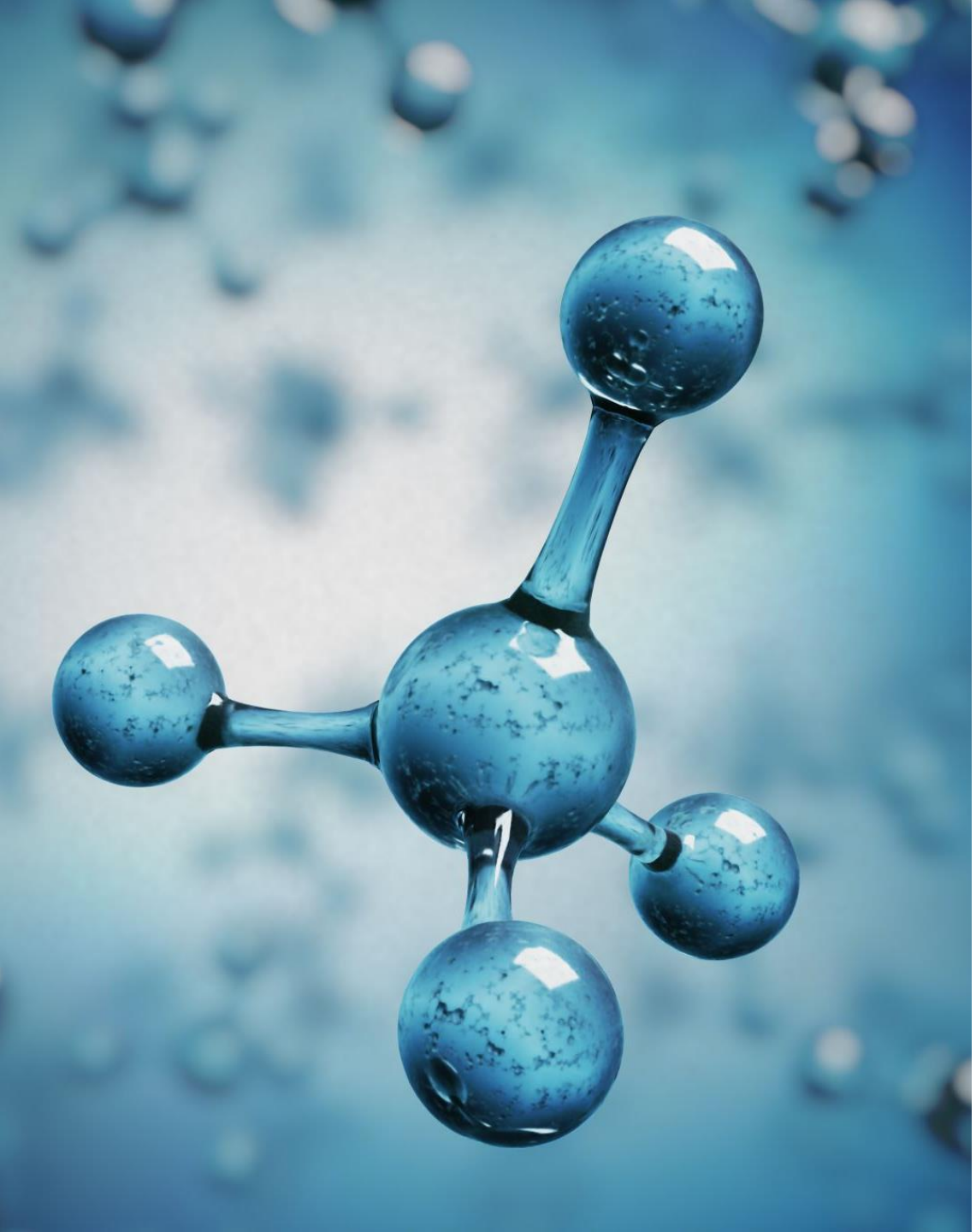

Molecular Qubits

- So, one of the characteristics we want in a molecular spin qubit is that it is easy to achieve a spin state. Coordination compounds of transition metals such as Cr, Cu, Ni, V etc. can be selected to have unpaired spins.
- Another characteristic is that we want to maximize the time it can spend in the targeted coherent superpositions of qubits. Since there can be an I* S interaction between nuclear spins (I) and the electron spin (S) of the transition metal , this interaction can result in a decoherence of the qubit state. By designing molecular qubits such that atoms with net or strong nuclear spins are further from the transition metal atom we should improve the coherence time of the qubit.
- The stiffness of the lattice can also be a factor. A stiffer lattice generally means higher phonon energies. The higher energies are less likely to interact and cause decoherence of the qubit.
- Qubits that have better coherence times at high temperatures are of interest because this could result in a less costly quantum computer. So good room temperature coherence is a desired objective.

Molecular Qubits

- One type of molecule proposed as a qubit with better room temperature coherence are copper(II) complexes.
    - Room Temperature Quantum Coherence in a Potential Molecular Qubit.

      NATURE COMMUNICATIONS , 5:5304 , DOI: 10.1038/ncomms6304 , www.nature.com/naturecommunications
- An analog for one of these molecules has been studied to better understand the electronic states of the molecule, focusing on the lower lying states which are of most interest in the dynamics of the qubit behavior .
    - Characterizing Excited States of a Copper Based Molecular Qubit Candidate with Correlated Electronic Structure Methods.

      J. Phys. Chem. A 2023, 127, 6764-6770
- The following does initial calculations on the copper qubit analog studied in the last paper.

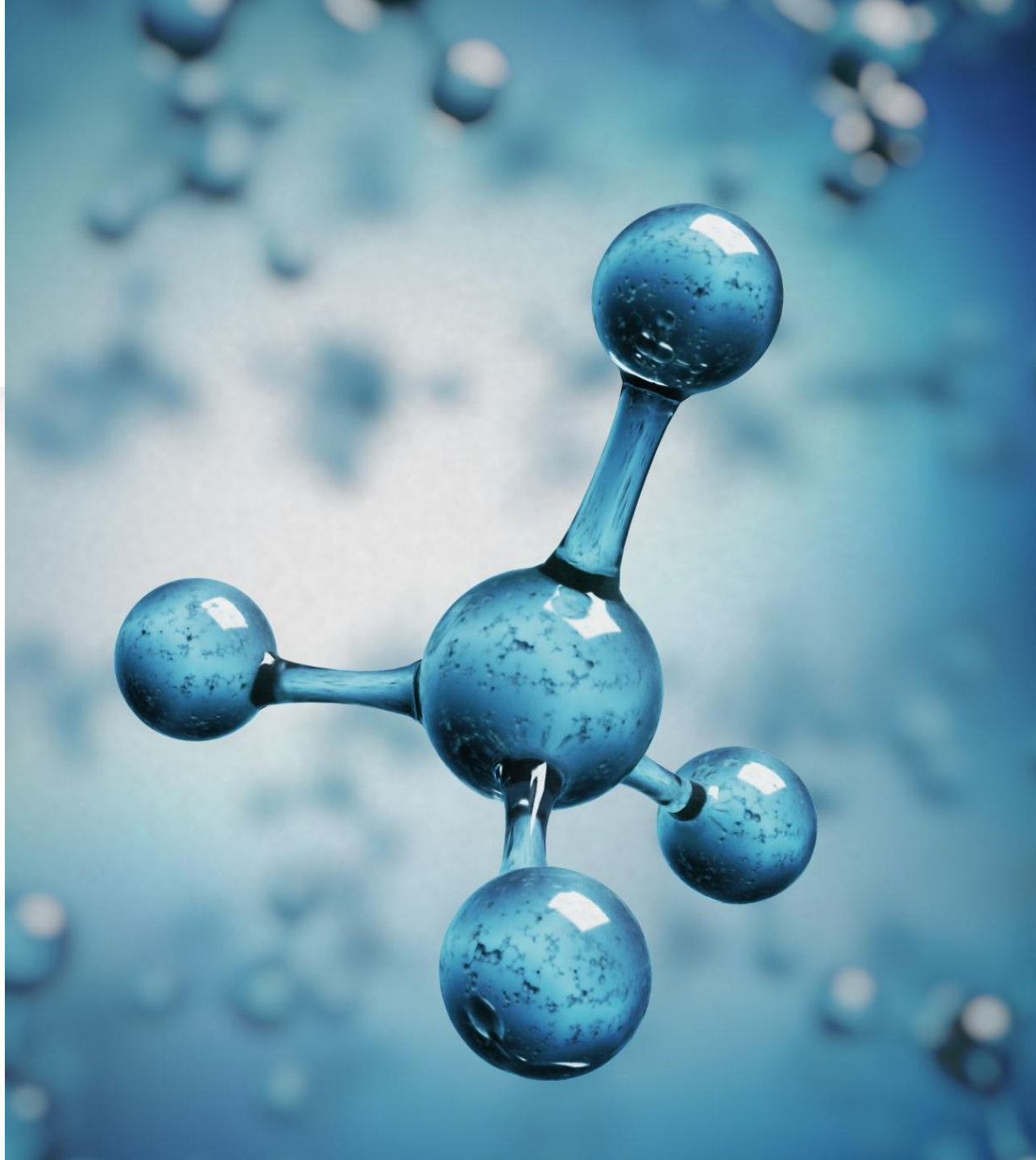

Room Temperature Copper Qubit Article Extracts

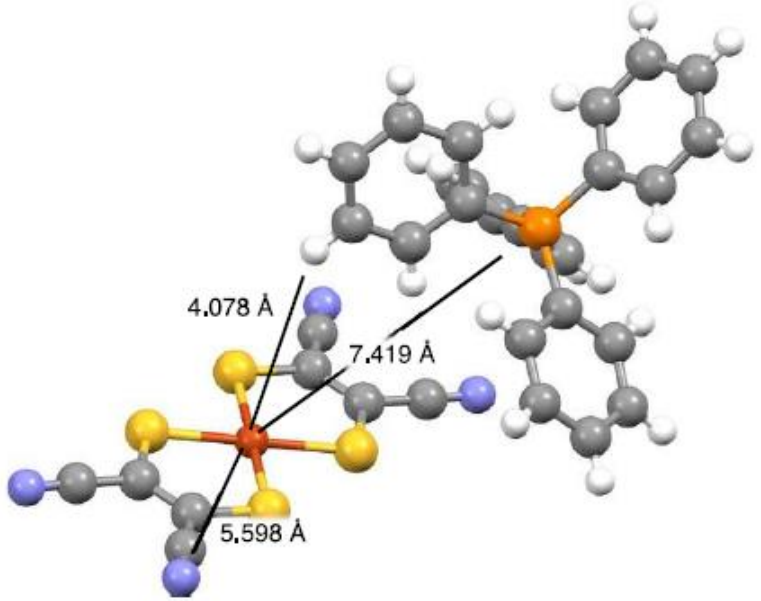

Figure 1 | Structure of 1Cu. Distances between the metal ion and the nearest nuclei with nonzero spins are indicated in Å. Colours: copper-brown, sulfur-yellow, carbon-grey, nitrogen-blue, phosphorus-orange and hydrogen-white.

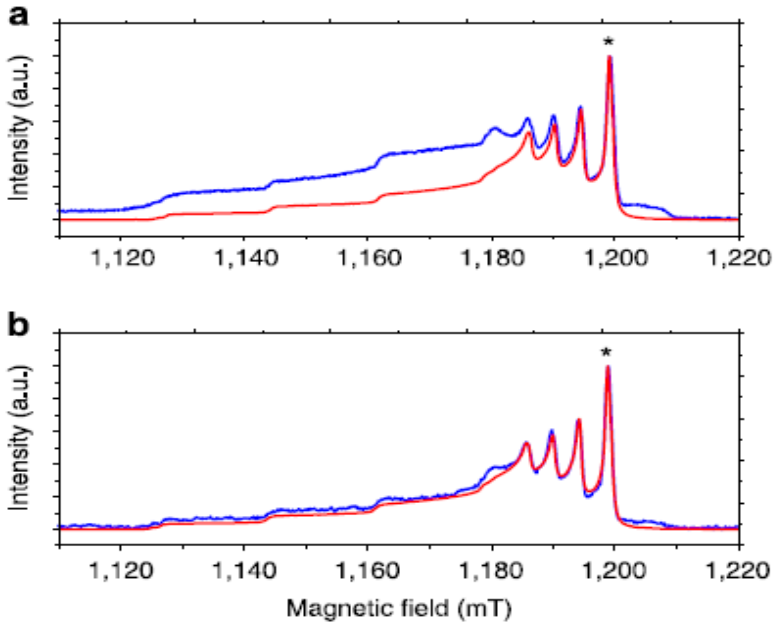

Figure 2 | ESE-detected Q-band EPR spectra of compound $1Cu_{0.001\%}$. Experimental results for EPR spectra (blue) recorded at $T = 7$ K (**a**) and $T = 120$ K (**b**), and simulation (red) using parameters given in the text.

These pictures show extracts from the article about a Room Temperature Cu qubit . Fig.1 shows the structure of the molecule studied and some interatomic distances. The copper is in an essentially square planar geometric configuration. Fig. 2 shows the Electron Paramagnetic Resonance (EPR) spectrum and simulation fits to the spectrum at two different temperatures. The spectrum is shown as a function of the applied magnetic field. Typically, a fixed RF/Microwave frequency is used and as the magnetic field is varied the energy differences go in and out of resonance with the electromagnetic radiation. Spectral finer details are related to the Cu atom spin and its couplings to nuclear spins.

Room Temperature Copper Qubit Article Extracts

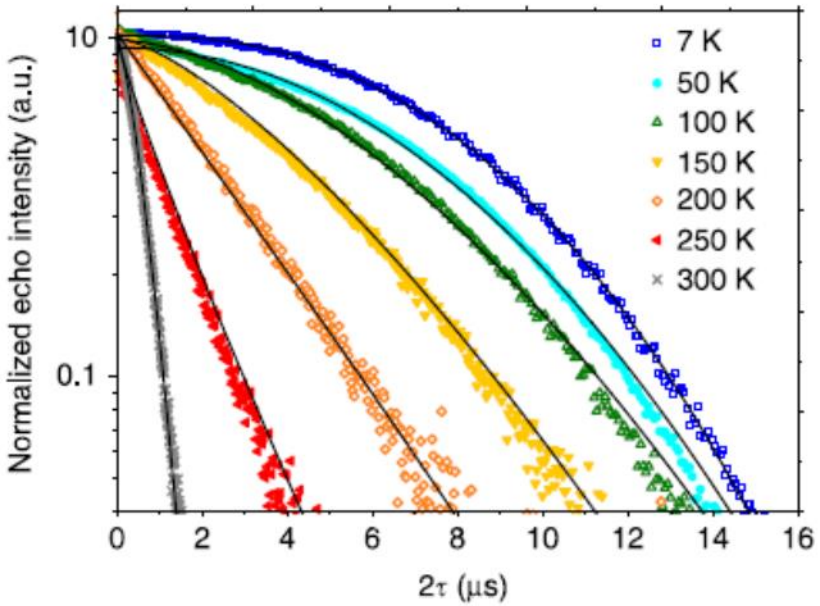

Figure 3 | Hahn echo decay curves at different temperatures for compound $1Cu_{0.001\%}$. Integrated echo intensity normalized to the echo intensity immediately after the spectrometer deadtime as a function of delay between initial pulse and echo, at various temperatures as indicated. Solid lines are fits using equation (1), see text.

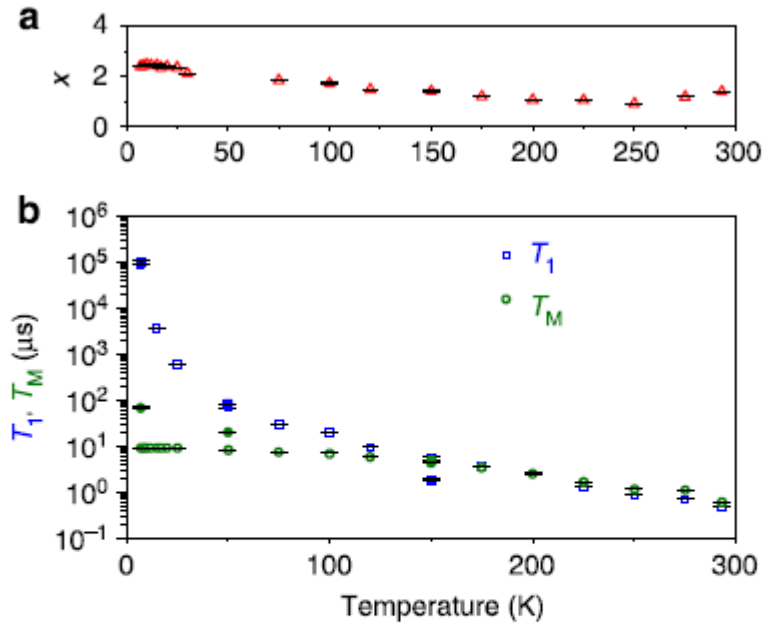

Figure 4 | Temperature dependence of electron spin relaxation times. (**a**) Stretch factor x as a function of temperature ($1Cu_{0.001\%}$ only). (**b**) Spin–lattice relaxation (T_1) and phase memory time (T_M) as a function of temperature. Open symbols belong to $1Cu_{0.001\%}$, filled symbols belong to $1Cu_{0.01\%}D$. Error bars in all panels correspond to the s.d. of the fits.

Presence of a spin echo in an EPR experiment is an indicator of coherence. This data shows that the coherence is much better at low temperatures but that some coherence is maintained for a time period of about 1 usec even at room temperature.

Methods Used in Room Temperature Copper Qubit Article

EPR measurements. CW X-Band EPR spectra were recorded on a Bruker EMX spectrometer ($\nu = 9.47$ GHz, Stuttgart). Pulsed EPR measurements were performed with a Bruker Elexsys E580 at Q-band ($\nu = 34$ GHz, Frankfurt, $\mathbf{1Cu_{0.001\%}}$) and a home-built[44] pulsed Q-band spectrometer ($\nu = 35$ GHz, Stuttgart, $\mathbf{1Cu_{0.01\%}D}$ and $\mathbf{1Cu_{1.5\%}}$). Temperatures between 7 and 275 K were obtained with an Oxford Instruments CF935 continuous flow helium cryostat, room temperature measurements were done at ~294 K without external temperature regulation. Typical pulse lengths were 16 ns ($\pi/2$) and 32 ns (π) (Frankfurt) and 20 ns ($\pi/2$) and 40 ns (π) (Stuttgart). For ESE-detected EPR spectra, the Hahn Echo pulse sequence ($\pi/2$—τ—π—τ—echo) with fixed delay times of $\tau = 140$ and 160 ns at 7 and 120 K, respectively, were applied under sweeping the magnetic field. Phase memory times were measured also with Hahn echo sequence, here at a fixed magnetic field under variation of the delay time τ. For measuring spin–lattice-relaxation times, the inversion recovery sequence (π—T—$\pi/2$—τ_{fix}—π—τ_{fix}—echo) with $\tau_{fix} = 140$ ns and phase cycling was applied. Nutation measurements were performed with a nutation pulse of variable length followed by a Hahn echo sequence (nutation pulse-τ_{nut}—$\pi/2$—τ_{fix}—π—τ_{fix}—echo) with $\tau_{nut} = 400$ ns, $\tau_{fix} = 140$ ns and different pulse powers.

Data analysis and simulation. ESE-detected spectra were simulated with EasySpin[45]. Errors of fit parameters (g and hyperfine values) were estimated by eye. T_M relaxation data were normalized to the first measurement point and fitted with Origin, indicated deviations correspond to the standard errors. Phase memory times (T_M) were extracted from fitting (stretched) exponentials, equation (1), to the Hahn echo decay curves. Experimental data of inversion recovery were fitted with a biexponential function for 7–25 K (fast and slow components) and for higher temperatures mono-exponential fits were applied.

Cu Qubit Analog

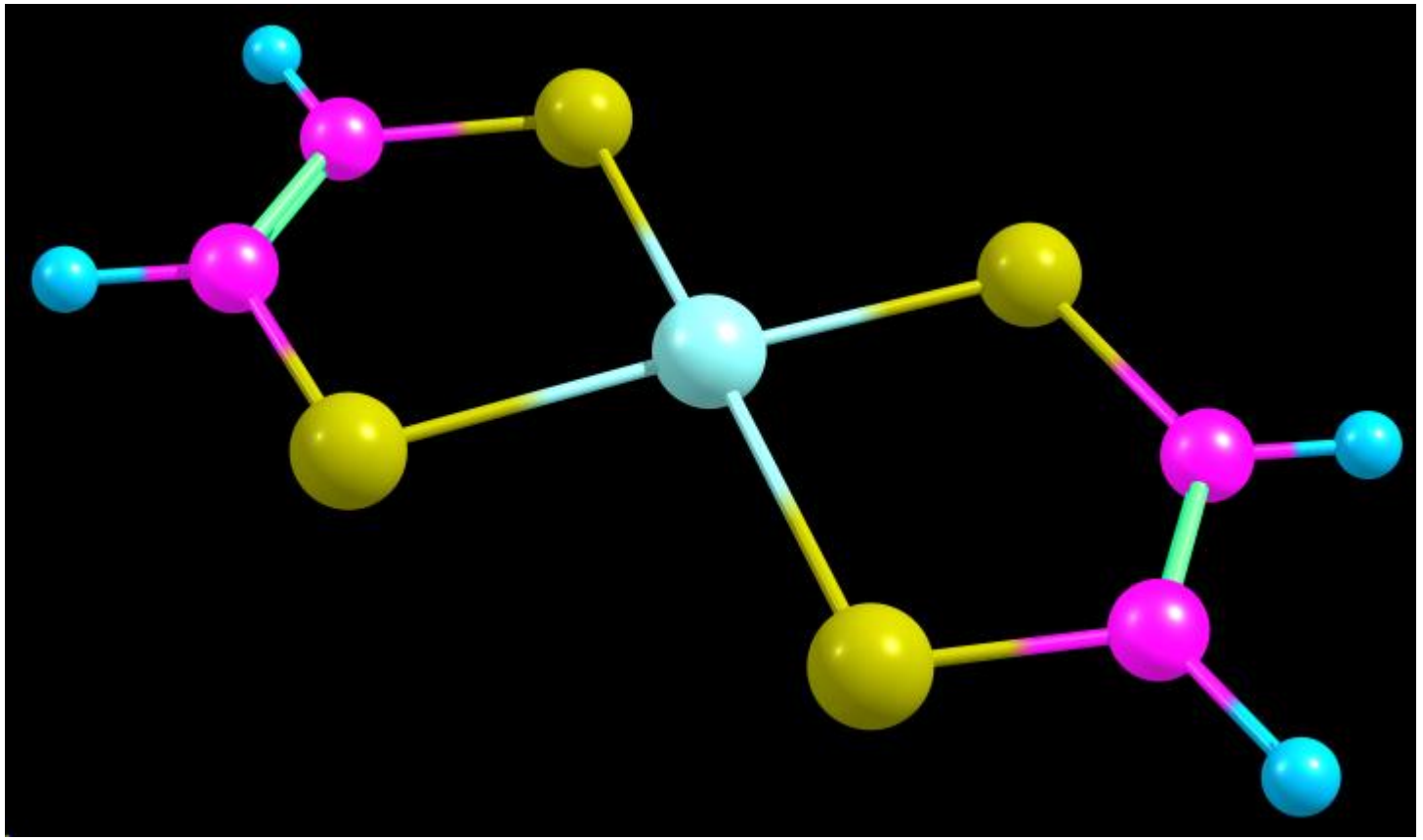

This molecule is an analog for a proposed room temperature molecular qubit. $[Cu(II)S_4C_4H_4]^{-2}$

The proposed molecule to which this is an analog has four cyano or N3 groups instead of the four hydrogens. The carbon atoms have no net nuclear spin (as opposed to the hydrogens). The nitrogen has a very weal spin intereaction. They therefore will have less interaction with the Cu(II) spin, reducing environmental interaction of the qubit.

However, the addition of additional electrons from the four cyano or N3 groups significantly adds computational complexity to quantum calculations, So this molecule is easier to study.

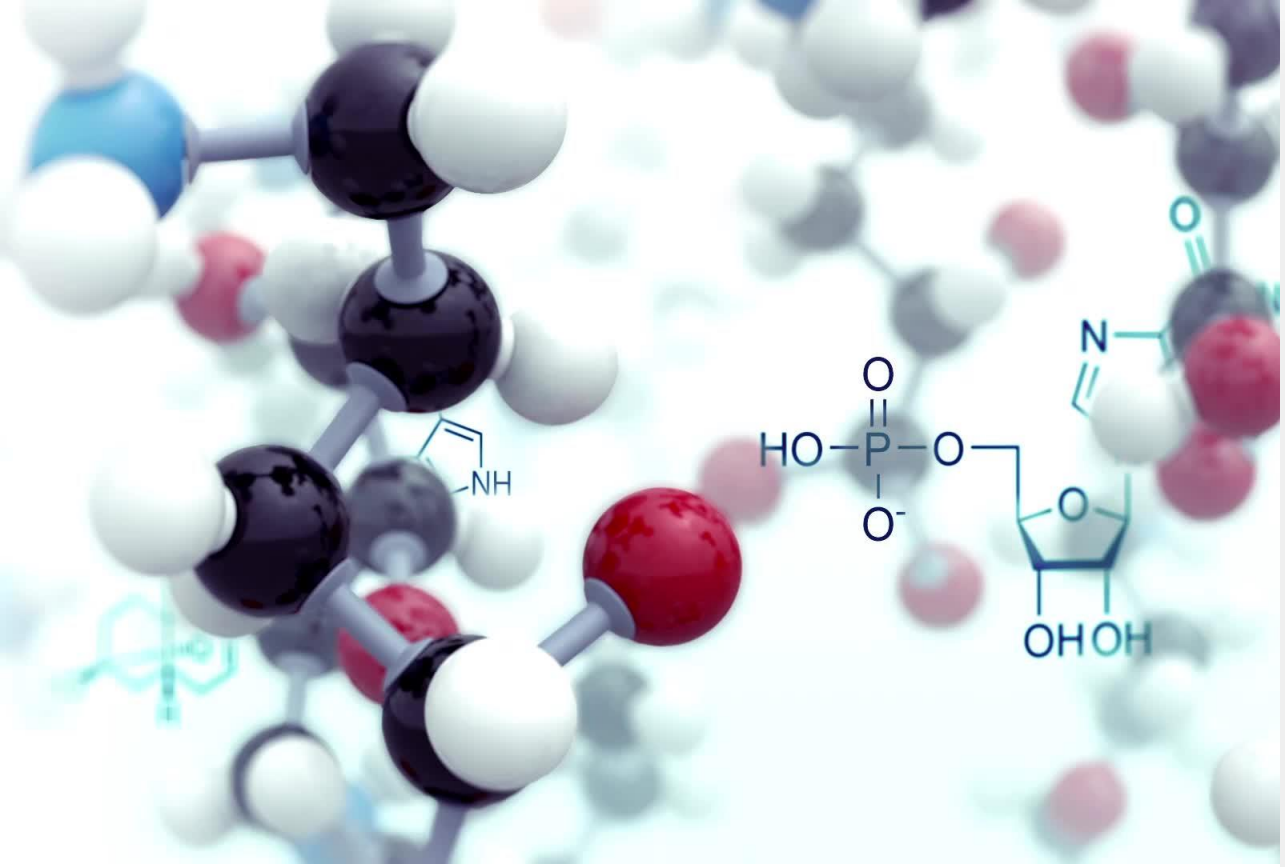

Calculations

- The molecule examined is an analog for a proposed room temperature molecular qubit. $[Cu(II)S_4C_4H_4]^{-2}$, or $[Cu(II)(edt)_2]^{-2}$ where edt is short for ethylene dithiolate a doubly negatively charged ligand.
- The Cu qubit analog molecule was geometry optimized using a DFT method with the PBEO functional, a basis set of def2/TZVPPD and the auxillary basis set def2/J.
- The molecule was drawn and initially optimized using Spartan 20.
- The resulting data was used to generate an XYZ file that was edited to be suitable for ORCA.
- The DFT calculation was done using ORCA 5.04.

ORCA Input File

- ! PBE0 def2-TZVPPD def2/J OPT
- !LargePrint NormalSCF PAL8 Printbasis PrintMOs

- * xyz -2 2
- Cu 0.79423 0.71870 0.00000
- S -1.02180 2.16851 -0.00000
- S 2.14846 2.60707 -0.00000
- S 2.61024 -0.73113 -0.00000
- S -0.55997 -1.16969 -0.00000
- C -2.35657 0.98041 -0.00000
- C -2.16717 -0.38861 -0.00000
- C 3.75565 1.82598 -0.00000
- C 3.94504 0.45693 -0.00000
- H 4.95690 0.07356 0.00000
- H 4.62545 2.46965 0.00000
- H -3.36845 1.36378 0.00000
- H -3.03696 -1.03230 0.00000
- *

This file shows that the ORCA computational chemistry calculation was done using

- A Density Functional Theory (DFT) functional of PBE0
- A basis set of def2-TZVPPD (triple zeta level)
- An auxillary basis set of def2/J

The calculation itself was a geometry optimization (keyword = OPT)

The calculation was done using 8 threads of parallel processing (keyword = PAL8)

The other comments refer to the data printed in the output file to be consistent with what ChemCraft software requires for input to that program for visualization of the Molecular Orbitals.

The atomic position are given by the XYZ file in angstroms

The net charge on the molecule is -2
The multiplicity of 2S+1 is 2, since the spin S is ½.

Graphical Representations of Molecular Orbitals

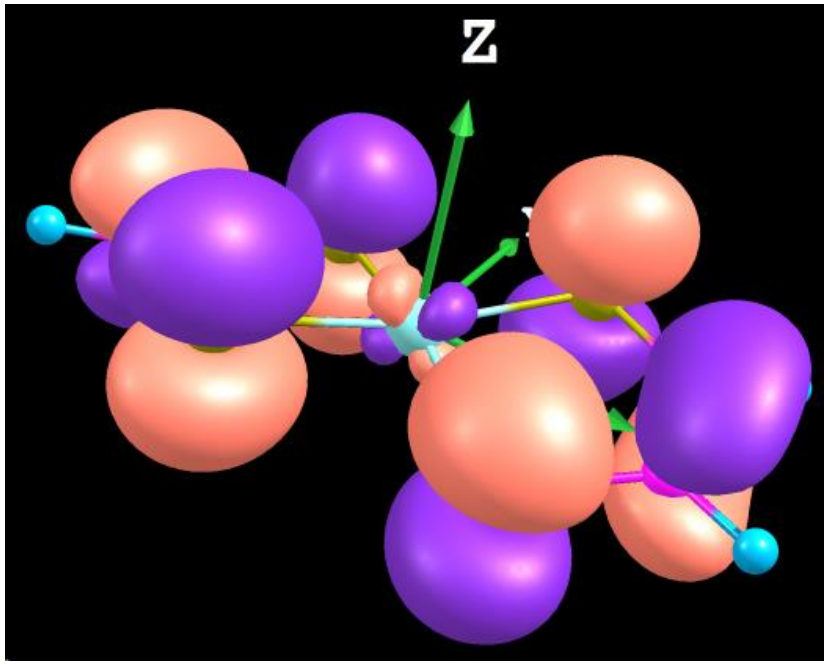

This is the Highest Occupied Molecular Orbital (HOMO) for the Cu(II) molecule as calculated.
Energy=0.0941 a.u. (Hartrees)
or 2.5606 eV
Note the d_{xz} character around the Cu atom

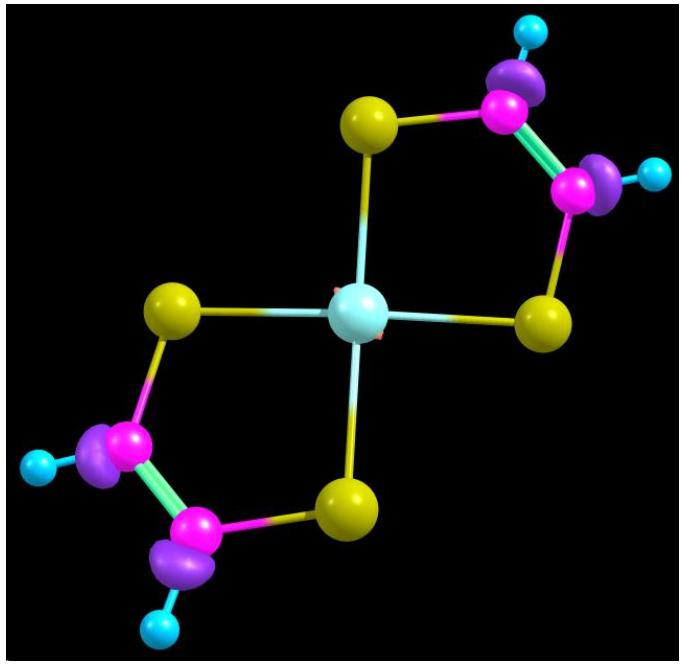

This is the Lowest Unoccupied Molecular Orbital (LUMO) for the Cu(II) molecule as calculated.
Energy=0.1991 a.u. (Hartrees)
Or 5.4178 eV

A HOMO -> LUMO transition would be 2.8572 eV , or 23,044 cm-1 , or 434 nm

$Cr(o\text{-}tolyl)_4^{+3}$ Optmized Geometry

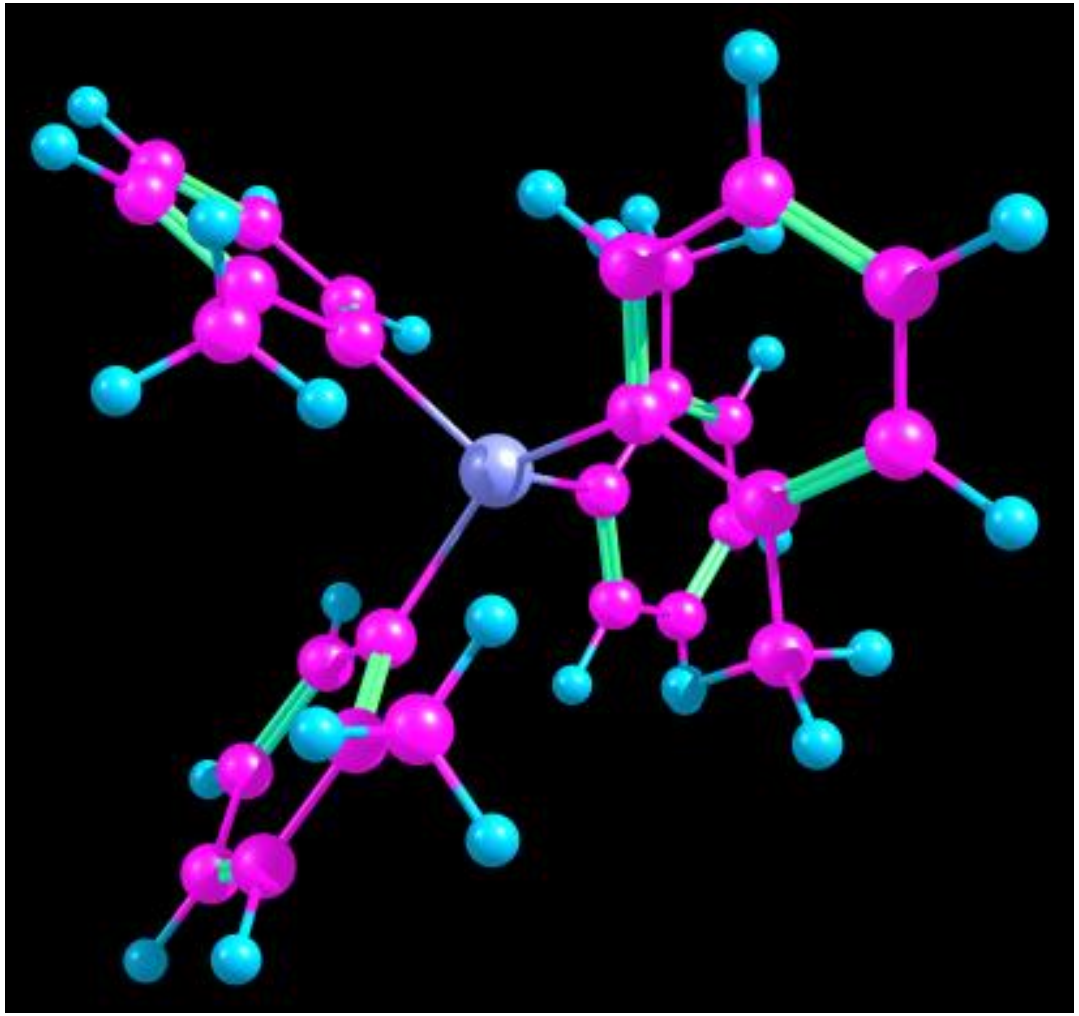

Another class of molecules being examined as potential moilecular spin qubits is the family of pseudo tetrahedral Cr(III) complexes with eother aryl or alkyl ligands.

Here we are looking at the Cr(III) complex with four ortho-tolyl aryl ligands.

We examine this molecule with some DFT and TDDFT/TDA calculations.

ORCA Input File- Cr(o-tolyl)4.inp

1> ! BP86 def2-SVP def2/J TightSCF # DFT method, Basis Set, Auxillary Basis Set and Convergence Target

2> ! PAL8 Largeprint Printbasis PrintMOs # Parallel processing of 8 threads, Print output for Chemcraft

3> %maxcore 1000 # Memory settings often need to be modified when running TDDFT. Check batching info in the TDDFT output.

4> %tddft #Call the Time Dependent Density Functional Theory method, Tamm-Dancoff Approximation is the default

5> nroots 15 # Setting the number of roots (transitions) to be calculated.

6> maxdim 5 # Davidson expansion space = MaxDim * nroots. Use MaxDim 5-10 for favorable convergence. Note that the larger MaxDim is, the more disk space is required

7> end

Geometry Part of Input File

MO Energies

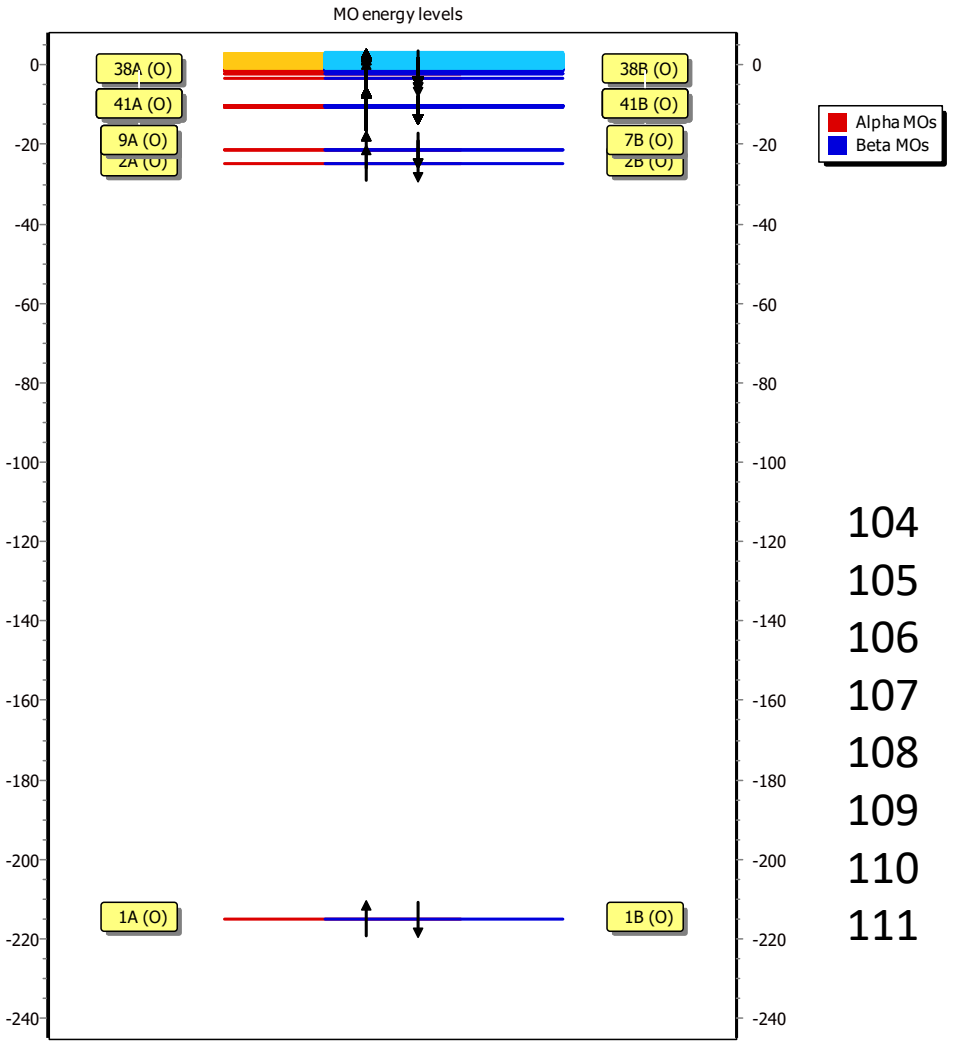

MO Energies in Vicinity of HOMO-LUMO Transition

Alpha Orbitals			Beta Orbitals		
104	-0.70904	Occupied	104	-0.70352	Occupied
105	-0.70684	Occupied	105	-0.70135	Occupied
106	-0.70167	Occupied	106	-0.69293	Occupied
107	-0.70018	Occupied	107	-0.68487	Occupied
108	-0.69971	Occupied	108	-0.67538	Unoccupied
109	-0.69732	Occupied	109	-0.67415	Unoccupied
110	-0.62579	Unoccupied	110	-0.67187	Unoccupied
111	-0.60898	Unoccupied	111	-0.66012	Unoccupied

First 10 Absorption Transitions of $Cr(o\text{-tolyl})_4^{+3}$

ABSORPTION SPECTRUM VIA TRANSITION ELECTRIC DIPOLE MOMENTS

State	Energy (cm-1)	Wavelength (nm)	fosc	T2 (au**2)	TX (au)	TY (au)	TZ (au)
1	3715.0	2691.8	0.003873705	0.34327	0.09039	-0.05794	0.57597
2	3915.2	2554.2	0.005134235	0.43172	0.50106	0.42113	0.05756
3	4474.3	2235.0	0.007958722	0.58559	0.12628	0.31686	-0.68501
4	4539.1	2203.1	0.006035635	0.43776	0.21631	0.14773	0.60757
5	4807.5	2080.1	0.028613366	1.95939	-1.33380	-0.01178	0.42455
6	5411.0	1848.1	0.018458838	1.12306	0.41874	-0.96507	-0.12791
7	5905.7	1693.3	0.003672306	0.20471	0.42672	-0.11646	0.09516
8	6132.1	1630.8	0.001915106	0.10282	-0.10618	-0.15621	-0.25911
9	6379.9	1567.4	0.003059722	0.15789	-0.20249	0.33560	-0.06524
10	6516.6	1534.5	0.001072273	0.05417	0.23082	-0.02384	0.01802

Lowest Energy Electronic Transitions for +4 charged Cr(o-tolyl)4

Wavelength(nm)	Oscillator Strength	MO Component	%	Orbital	
2430.18	0.0010	sHOMO-216 -> sLUMO	8%	alpha	m=2.24
2632.55	0.0007	HOMO-2 -> LUMO	49%	alpha	m=2.24
		HOMO-3 -> LUMO	29%	alpha	
3120.78	0.0058	sHOMO-216 -> sLUMO	36%	alpha	m=2.24
		sHOMO-216 -> sLUMO	35%	alpha	
3252.41	0.0020	sHOMO-216 -> sLUMO	41%	alpha	m=2.24
		HOMO-2 -> LUMO	22%	alpha	
		sHOMO-216 -> sLUMO	18%	alpha	
4095.32	0.0030	sHOMO-216 -> sLUMO	9%	alpha	m=2.24
6327.75	0.0015	sHOMO-216 -> sLUMO	38%	alpha	m=2.24

Partial Absorption Spectrum-Spartan Calc

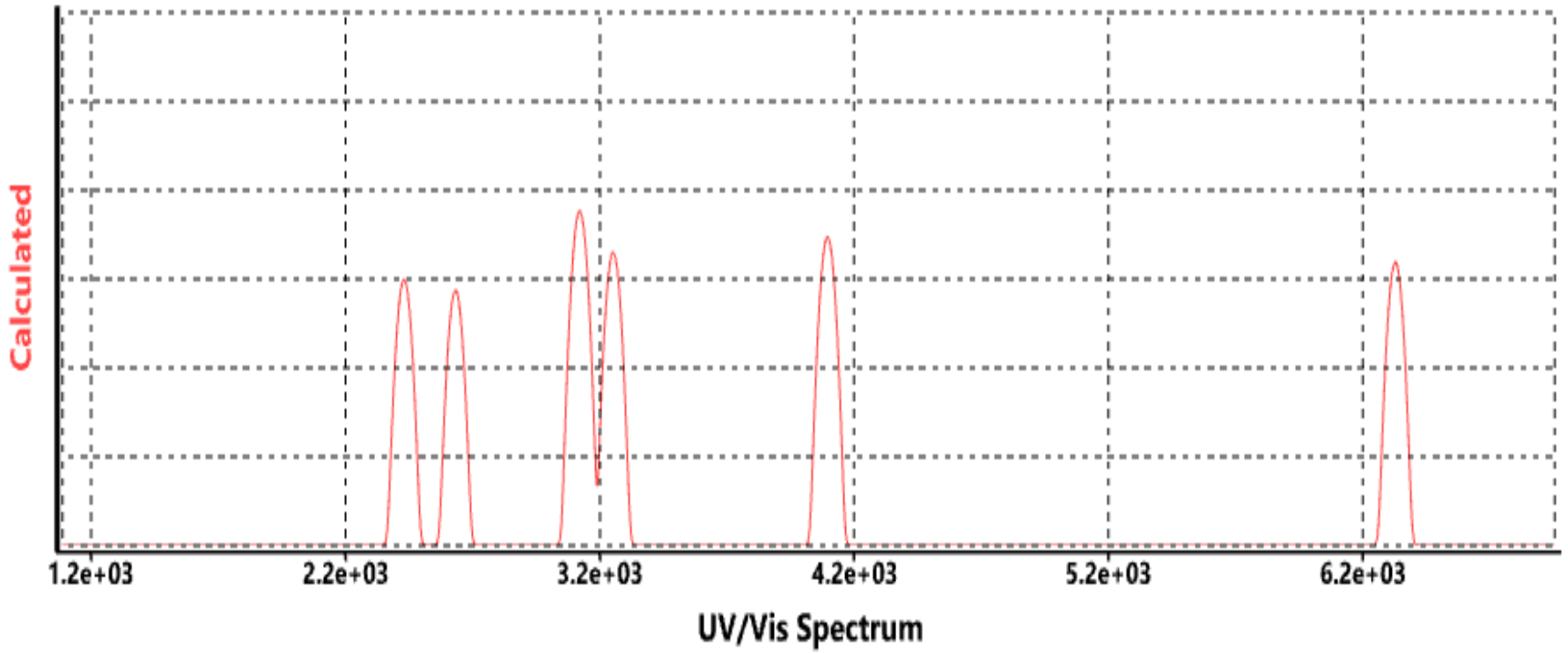

Electronic Transitions for Neutral Cr(o-o-xylyl)4

		strength		MO Component		%	
	495.82	0.0088		sHOMO-252 -> sLUMO+2	93%	alpha	m=2.24
	537.49	0.0073		sHOMO-252 -> sLUMO+1	92%	alpha	m=2.24
	589.99	0.0063		sHOMO-252 -> sLUMO+2	95%	alpha	m=2.24
	625.47	0.0021		sHOMO-252 -> sLUMO	78%	alpha	m=2.24
				sHOMO-252 -> sLUMO+1	17%	alpha	
	638.47	0.0092		sHOMO-252 -> sLUMO+1	74%	alpha	m=2.24
				sHOMO-252 -> sLUMO	19%	alpha	
	691.17	0.0155		sHOMO-252 -> sLUMO	93%	alpha	m=2.24

Electronic Spectrum for Neutral Cr(o-o-xylyl)4

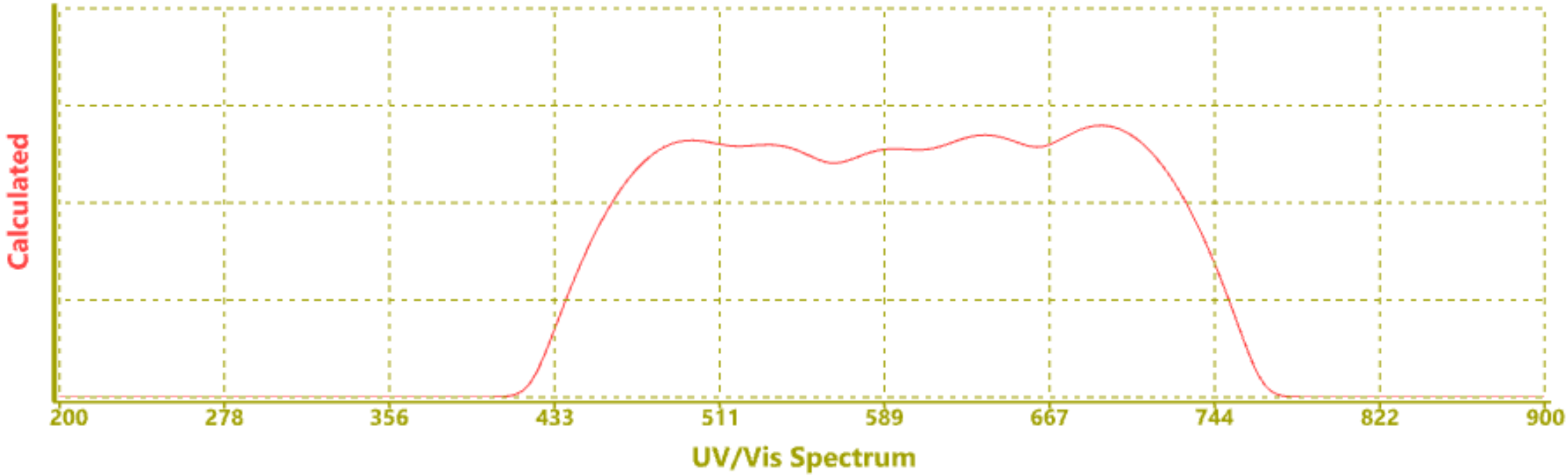

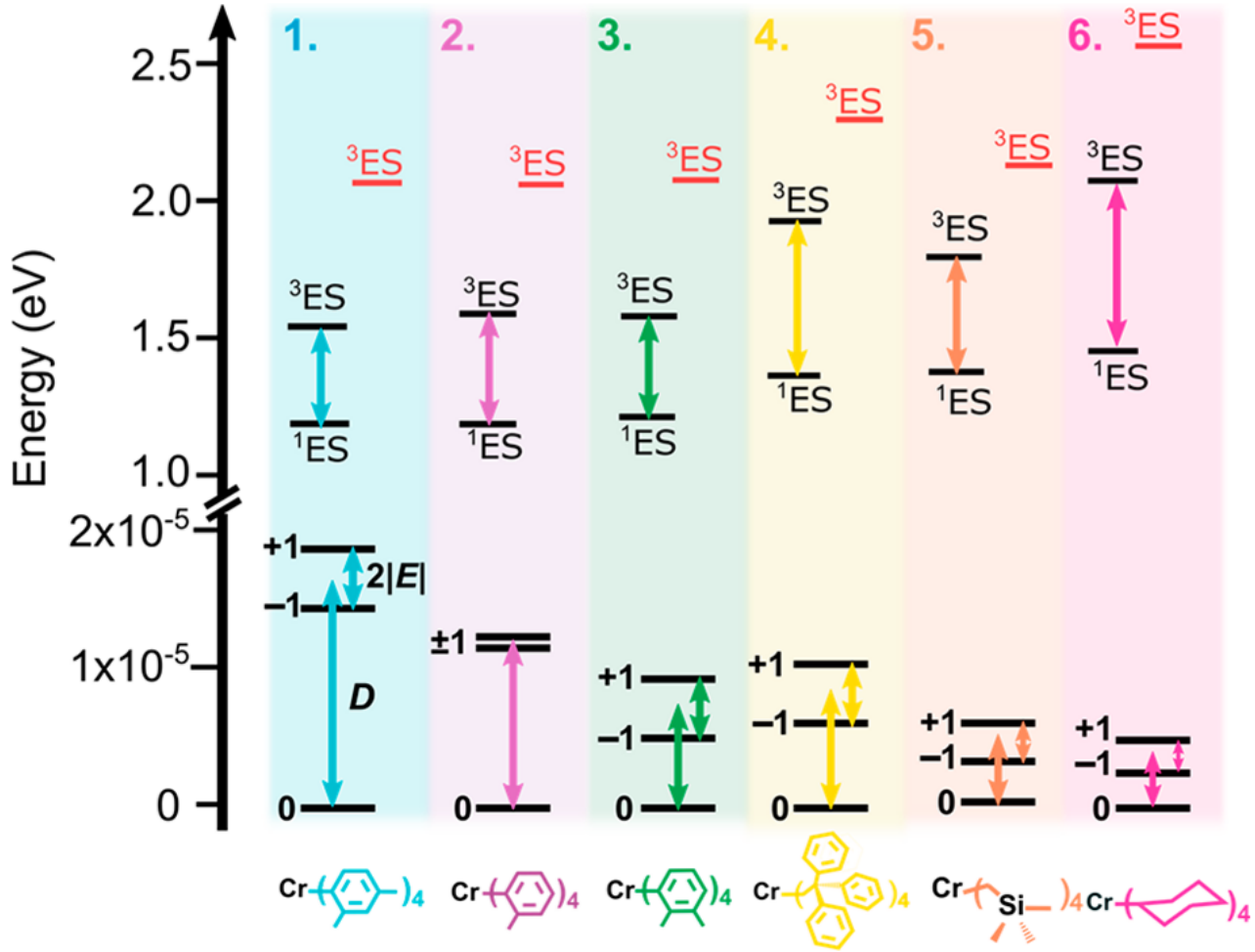

Figure 8. Overall energy level diagram for **1**–**6**. ZFS values were determined from cw-EPR experiments at 77 K, and the experimental excited states (black) were approximated from PL experiments at 4 K and from the deconvolution of the UV–vis–NIR absorption spectra in Figure S17. The first TDDFT spin-triplet excitation energies are given in red.

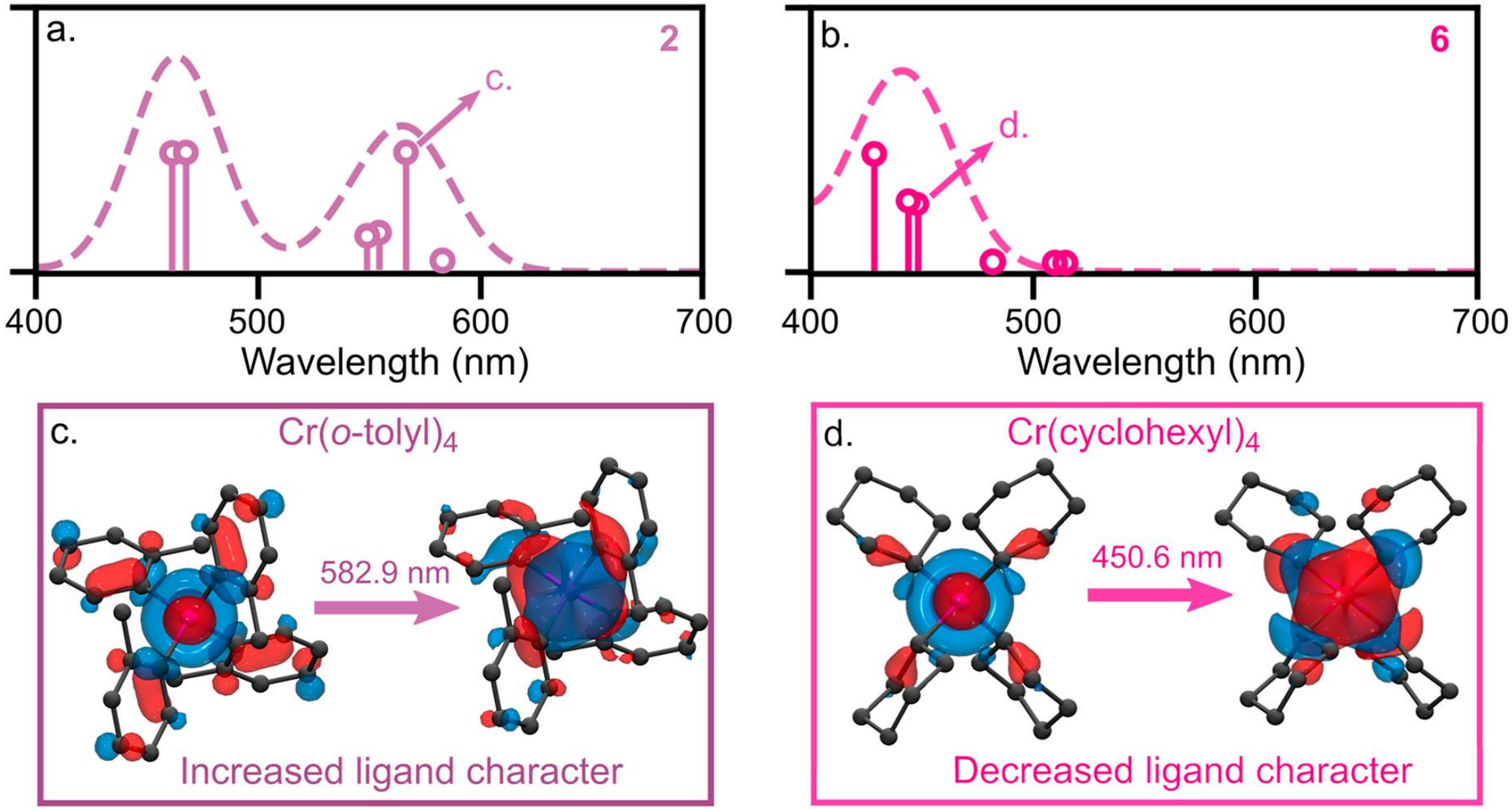

Figure 7. (a, b) Normalized TDDFT absorption spectra of **2** (a) and **6** (b) with a Gaussian broadening width of σ = 20 nm. Excitations with relative oscillator strengths are given as sticks. (c, d) NTOs with contributions >96% for the second and fourth spin-triplet excitations of **2** (c) and **6** (d) indicated by arrows on the calculated absorbance spectra. For each excitation, the "hole" and "electron" orbitals are given on the left and right of the arrow, respectively.

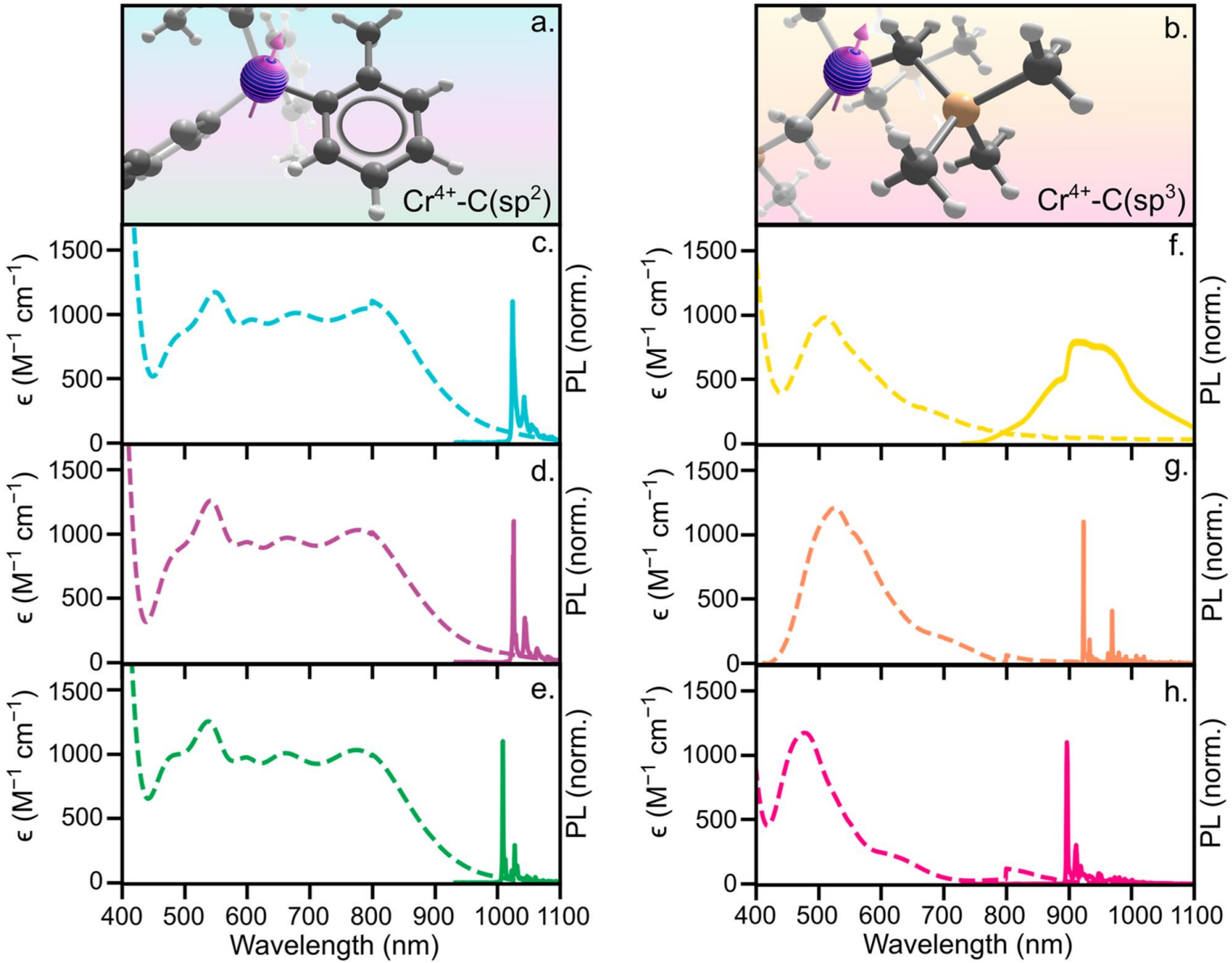

Figure 6. (a, b) Molecular structures of **2** (a) and **5** (b) highlighting the variation in metal−ligand bonding between Cr−aryl and Cr−alkyl systems with Cr, C, Si, and H given as purple, gray, peach, and white, respectively. (c−h) Room temperature UV−vis−NIR spectra in toluene (dashed lines) and 4 K PL spectra in diluted solid state, Sn matrix (solid lines) of **1** (c), **2** (d), **3** (e), **4** (f), **5** (g), and **6** (h). PL spectra were measured following excitation of **1′**−**3′** and **4′**−**6′** at 785 and 660 nm, respectively.

$Cr(IV)(o\text{-}tolyl)_4$ Structure

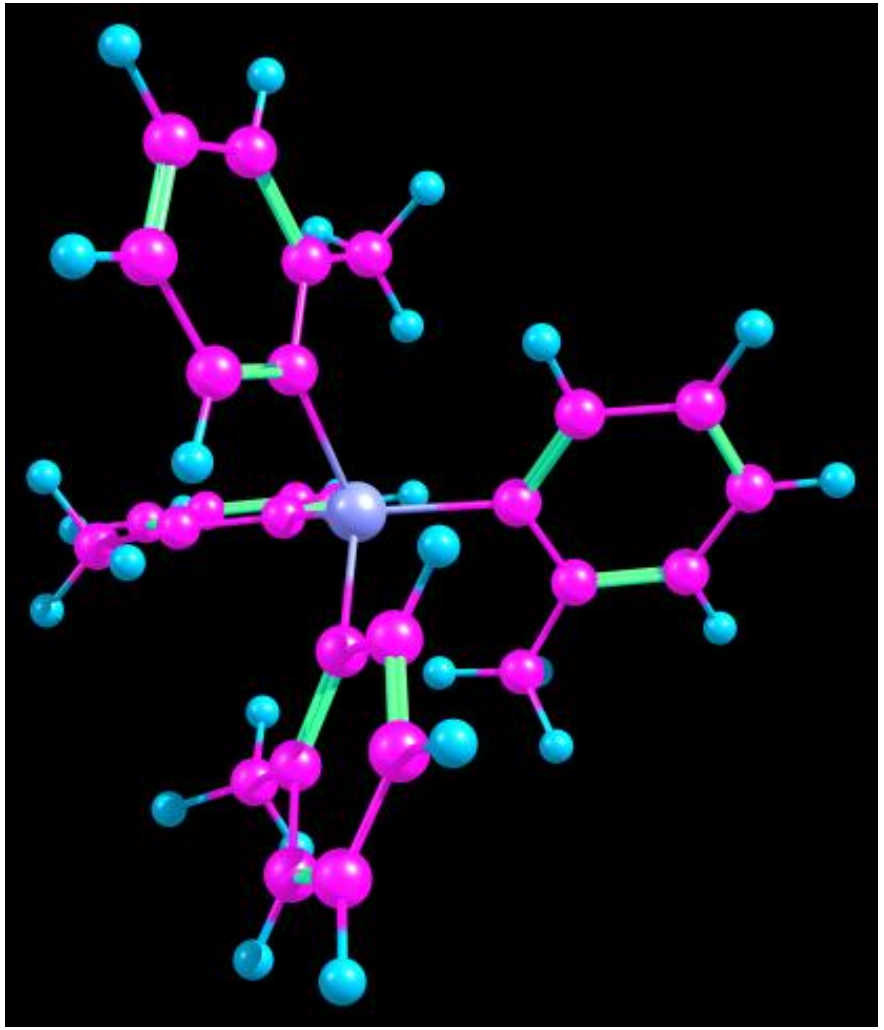

Spin Density Plot for $Cr(o\text{-}tolyl)_4^{+3}$

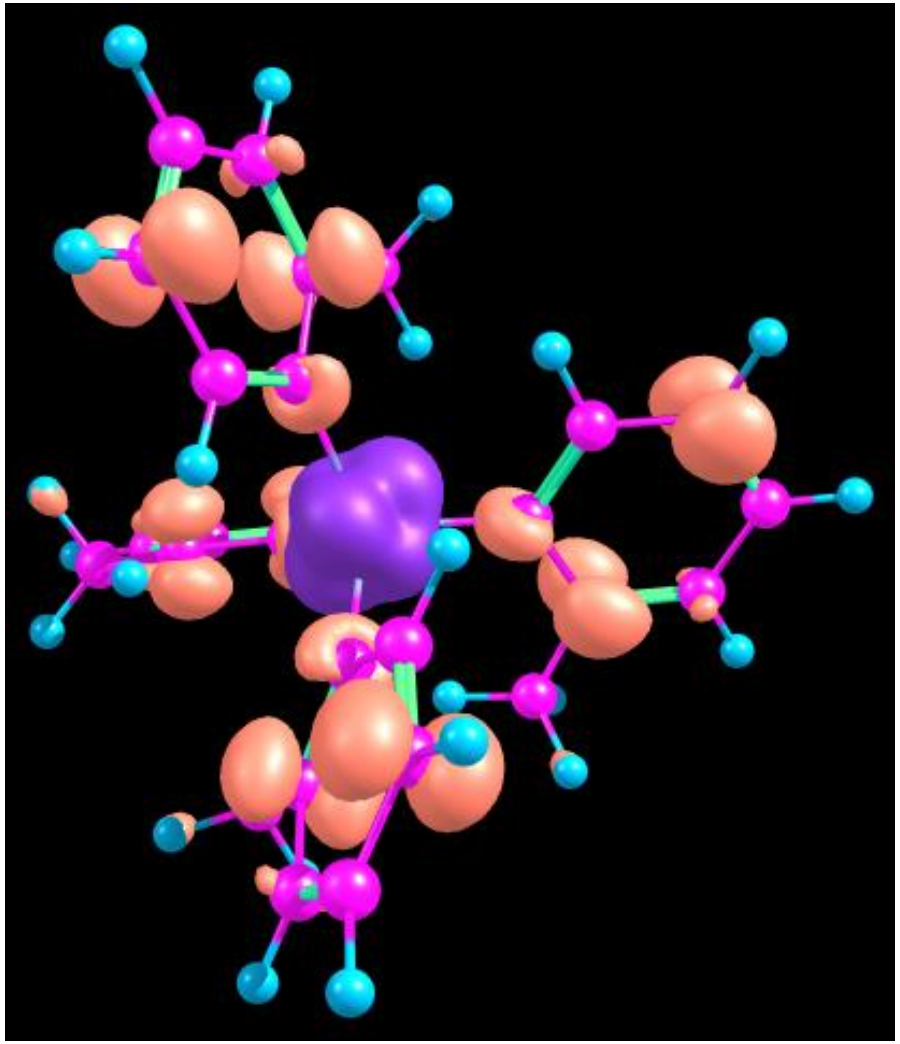

This is a plot of the spin density as calculated by summing the density of the occupied alpha electron (spin up) orbitals and subtracting the summed density of the occupied beta electron (spin down) orbitals.

Calculations of orbitals done using ORCA 5.04 software.

Plot done using Chemcraft software.

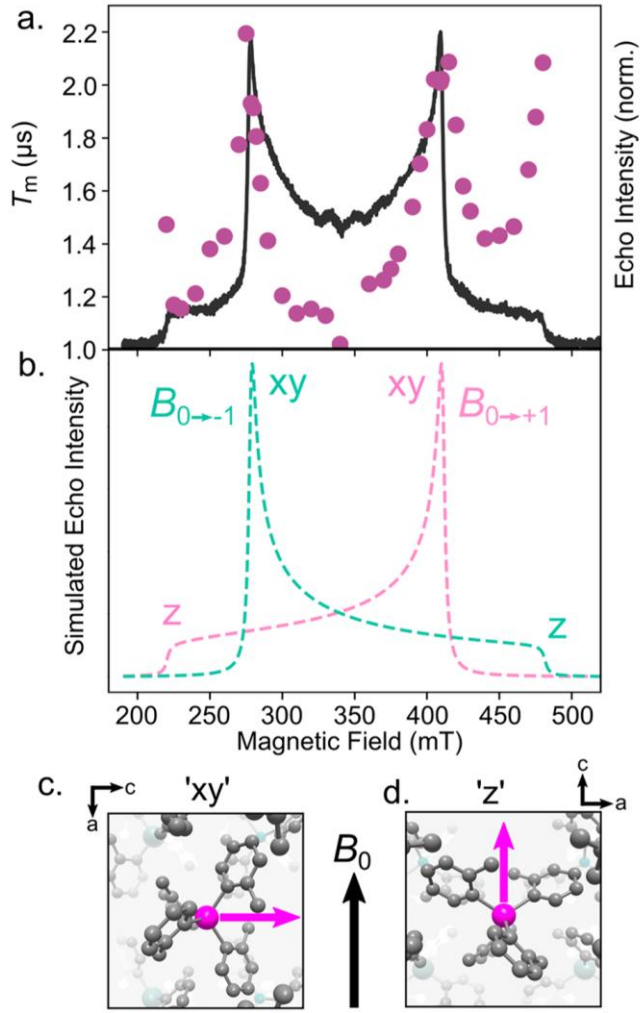

Figure 5. (a) X-Band magnetic field dependence of T_m (purple circles) for **2′** at 10 K overlaid on the corresponding echo-detected field swept spectrum (black). (b) Decomposition of transitions between $M_S = 0$ to $M_S = -1$ ($B_{0\rightarrow-1}$, green) and $M_S = 0$ to $M_S = +1$ ($B_{0\rightarrow+1}$, pink), the sum of which result in the EDFS spectrum in part a. (c, d) Crystallographic orientation of **2′** highlighting the principal axis of the ZFS tensor (pink arrow), aligned perpendicular (c) and parallel (d) to the external magnetic field, B_0 (black arrow). The crystallographic *a* and *c* axes are given for each orientation. See Figure S11 for the filled unit cell.